

Molybdenum-Rhenium alloy based high- Q superconducting microwave resonators

Vibhor Singh,* Ben H. Schneider, Sal J. Bosman, Evert P. J. Merkx, and Gary A. Steele

Kavli Institute of NanoScience, Delft University of Technology,

PO Box 5046, 2600 GA, Delft, The Netherlands.

(Dated: November 19, 2014)

Abstract

Superconducting microwave resonators (SMR) with high quality factors have become an important technology in a wide range of applications. Molybdenum-Rhenium (MoRe) is a disordered superconducting alloy with a noble surface chemistry and a relatively high transition temperature. These properties make it attractive for SMR applications, but characterization of MoRe SMR has not yet been reported. Here, we present the fabrication and characterization of SMR fabricated with a MoRe 60-40 alloy. At low drive powers, we observe internal quality-factors as high as 700,000. Temperature and power dependence of the internal quality-factors suggest the presence of the two level systems from the dielectric substrate dominating the internal loss at low temperatures. We further test the compatibility of these resonators with high temperature processes such as for carbon nanotube CVD growth, and their performance in the magnetic field, an important characterization for hybrid systems.

Molybdenum-Rhenium (MoRe) is an attractive superconducting alloy which has been explored as early as the 1960s¹⁻³. Recently, there has been a renewed interest in MoRe superconductors due to its electrical and mechanical properties⁴⁻⁷. Depending on the alloying ratio and film deposition temperatures, thin films of MoRe have shown superconducting transition temperatures (T_c) ranging from 8 K to 13 K and residual resistance ratios $RRR \approx 1$ indicating their highly disordered nature. Despite these attractive properties, it has not been explored as a material for the superconducting coplanar waveguide resonators. The High frequency and low dissipation of superconducting microwave resonators (SMR) have led to their use in a variety of applications ranging from sensitive photon detectors⁸, quantum computation^{9,10}, and coupling to nanoelectromechanical resonators¹¹. There has been also a considerable interest in combining them to DC electron transport devices based on carbon nanotubes¹², nanowires¹³, 2-dimensional electron gases^{14,15}, spin ensembles^{16,17}, and magnons¹⁸. These hybrid coupling devices require robustness of low dissipation in the SMR against the fabrication process (such as high-temperature growth) and the measurement scheme, such as in magnetic field. The versatile use of SMR and constraints for various applications have led to the studies of different superconductors¹⁹⁻²¹, where MoRe could be an attractive alternative.

The motivation for exploring MoRe for the SMR is multifold. Its highly disordered nature of MoRe makes it attractive for kinetic inductance detectors⁸. It makes highly transparent superconducting contacts with carbon nanotubes²² and has been used to make contact with graphene in forming a high quality-factor superconducting opto-mechanical device²³. Furthermore, a high upper critical magnetic field⁶ makes it attractive for applications requiring magnetic field. Here, we investigate SMR fabricated using a 60-40 alloy of MoRe. We provide a fabrication recipe to make superconducting microwave resonators with low dissipation, characterize their performance after a high temperature chemical vapor deposition process and in the presence of magnetic field.

The SMR were designed in a coplanar waveguide geometry and fabricated on a sapphire wafer (substrate thickness $\sim 430 \mu\text{m}$) in order to minimize dielectric losses. As cleaning of the substrate surface seems to play an important role in minimizing two-level systems²⁴, an extensive cleaning of the sapphire wafer is performed with phosphoric acid (H_3PO_4) at 75 °C for 30 minutes followed by rinsing in DI water for 2 hours. After exposing the fresh surface of the wafer, it was immediately loaded in the vacuum chamber for MoRe film

deposition. Using an RF sputtering system, we deposit a 145 nm thick MoRe film with a continuous flow of Ar (pressure 1.5×10^{-3} mTorr) from a ~ 99.95 % purity, single target of MoRe. The SMR designs were patterned using e-beam lithography on a three layer mask (S1813/W(Tungsten)/PMMA-950) followed by the etching of MoRe by SF₆/He plasma. We use a frequency multiplexing scheme to side-couple multiple quarter wavelength resonators of different frequencies to a common transmission line. Figure 1(a) shows an optical microscope image of such a resonator after the fabrication process. The quarter-wavelength coplanar waveguide resonator is formed by terminating a transmission line (characteristic impedance of 50 Ω and 10 μm wide trace) to the ground plane. For microwave measurements, the samples were mounted in a light-tight microwave box and were cooled down in a dilution fridge or a He-3 cryostat with sufficient attenuation at each temperature stage to thermalize the microwave photons reaching the sample. A schematic of the attenuation scheme in the dilution refrigerator is shown in Figure 1(b). For these sputtered thin films, we measure a typical room temperature resistivity of 88 $\mu\Omega\text{-cm}$, $RRR \sim 1.2$ and $T_c \sim 9.2$ K.

The low power transmission response S_{21} for a side-coupled quarter wavelength resonator near its resonance frequency f_0 can be modeled by

$$S_{21}(f) = \frac{S_{21}^{min} + 2iQ_l\delta f}{1 + 2iQ_l\delta f}, \quad (1)$$

where $S_{21}^{min} = Q_c/(Q_c + Q_i)$ is the swing in transmission at resonance, $\delta f = \frac{f-f_0}{f_0}$, $Q_l = Q_c \times Q_i/(Q_c + Q_i)$ is the loaded quality-factor, Q_c is the coupling quality-factor and Q_i is the internal quality-factor of the resonator. Figure 1(c) shows the measurement of the transmission coefficient S_{21} for a resonator along with the fitted curve at $T = 830$ mK. We observe an internal quality-factor of 700,000 at low probe powers, comparable to the best results using a highly optimized Al deposition²⁴.

Figure 2 shows the typical temperature dependence of the normalized resonance frequency shift $\Delta f/f_0 = \frac{f_0(T) - f_0(315 \text{ mK})}{f_0(315 \text{ mK})}$ and the internal quality factor Q_i for a resonator. With an increase in temperature above ~ 2 K, the reduced cooper-pair density in the superconductor presents a larger kinetic inductance resulting in a sharp drop of the resonator frequency as temperature approaches T_c as shown in Figure 2(a). The corresponding increase in the number of quasi-particles also leads to a sharp drop in the internal quality-factor of the resonator as shown in Figure 2(b). The frequency and internal quality-factor response with temperature in the vicinity of T_c can be very well described by the Mattis-Bardeen (M-B)

theory²⁵, which predicts $\Delta f/f_0 = \frac{\alpha}{2} \frac{\Delta\sigma_2}{\sigma_2}$ and $Q_i = \frac{2}{\alpha} \frac{\sigma_2}{\sigma_1}$, where α is the kinetic inductance fraction, σ_1 and σ_2 are the real and imaginary parts of the complex conductivity, respectively. Using the experimentally measured normal state resistivity and T_c , we estimated a surface inductance $L_s \sim 0.35$ pH for these films. The blue curve in Figure 2(a) and (b) shows the expected temperature dependence of the normalized resonance frequency shift and internal quality-factor calculated using the M-B theory with no free parameters. For temperatures below 2 K, the resonance frequency shift and saturation in the internal quality-factor are not captured by the M-B theory as it predicts no change in the resonance frequency for $T \ll T_c$ and exponentially large Q_i . In this temperature range, we measure a small increase in the resonance frequency as shown in the inset of Figure 2(a). This small positive shift is attributed to the presence of two-level systems (TLS) and can be written as $\frac{\Delta f}{f_0} = \frac{F}{2} \frac{\Delta\epsilon}{\epsilon}$, where F is a geometrical factor and ϵ is the dielectric constant dominated by the resonant interactions over the relaxation of two-level systems at low temperature^{26,27}. Correspondingly, Q_i saturates and follows a trend similar to the normalized resonance frequency shift indicating the presence of TLS. With a large number of probe photons, the damping from the TLS saturates and leads to an increase in the internal quality-factor as shown in the inset of Figure 2(b) (additional data provided in supplemental material (SM)²⁸).

After establishing the large quality-factors and role of the two level systems in these resonators, we explore the changes in characteristics of the resonators after a chemical vapor deposition process at high temperatures. In order to form hybrid systems with the SMR by coupling them to other materials like a carbon nanotube based quantum dots and mechanical resonators, often a high temperature growth process is required. To explore the compatibility of these microwave resonators with high-temperature growth processes, we subject them to a chemical vapor deposition (CVD) growth process used to grow carbon-nanotubes. A continuous hydrogen flow is present during this process. Once the oven temperature of 900 °C is reached, a methane (CH₄) flow was added for 10 minutes (see SM for details²⁸). After this process, the superconducting transition temperature of these films decreased to $T_c \sim 4.0$ K with a room temperature resistivity of 108 $\mu\Omega$ -cm. Figure 3 shows a typical change in resonator characteristics before and after high temperature annealing measured at 315 mK. For all resonators, we have observed an approximately 250 MHz decrease in the resonance frequency after annealing as shown in Figure 3(a). Such a decrease in the resonance frequency can be attributed to the increased kinetic inductance fraction due to

the degradation in the superconducting film quality. After this process, we also observe a reduction in the internal quality-factor of the resonator, shown in Figure 3(b). The larger drop of Q_i after annealing suggests increased dielectric losses in the sapphire substrate (additional data provided in supplemental material²⁸). We have also studied the effects of annealing the resonators in pure hydrogen at 900 °C, and find that the T_c of the film increases to 11.8 K (improving the quality of the superconducting film). However, annealing also lead to increased dielectric loss in the substrate (see SM for more details).

For various hybrid coupling schemes of microwave resonator to systems such as spin ensembles^{16,17}, magnons¹⁸, and nanotube SQUIDs²², a low dissipation of the SMR in a magnetic field is desirable. In a magnetic field, formation of flux vortices can lead to added dissipation^{29,30}. After characterizing the high temperature annealed resonators, we subject them to small magnetic fields up to ~ 4.5 mT. Figure 4(a) shows the resonance frequency of one of the resonator with magnetic field applied perpendicular to the sample surface at 4.2 K. The presence of the vortices adds a reactive part to the resonator’s microwave response and hence reduces its resonance frequency. This becomes quite evident by looking at the detailed measurement of the resonance frequency with small steps in the magnetic field. The incorporation of individual vortices is reflected as abrupt jumps in the resonance frequency as shown in the inset.

The formation of vortices not only adds a reactive part to the microwave response, but also adds a dissipative part to it. Figure 4(b) shows the plot of reduction in Q_i with magnetic field (corresponding to the same resonator as shown in Figure 4(a)). Application of the magnetic field opens up an extra dissipation channel due to the motion of vortices in response to the microwave field, and it is often characterized by a magnetic field dependent dissipation rate given by $Q_B^{-1} = Q_i^{-1}(B) - Q_i^{-1}(0)$ ^{29,30}. The inset of figure 4(b) shows the plot of the magnetic field contribution to the total dissipation rate, which is smaller than in the previously studied devices with similar geometry using rhenium²⁹. It should be noted here that the geometry of the SMR studied here has continuous ground plane metalization, which leads to a significant magnetic flux focusing between the central conductor and the ground plane. The susceptibility to the magnetic field can further be improved by making holes in the ground plane, which act as vortex pinning centers³¹⁻³³.

In summary, we presented a fabrication method of superconducting microwave resonators based on MoRe alloy and observe high internal quality-factors. We characterized its surface

impedance, role of the two-level systems and compatibility of these resonators with high temperature CVD processes. Post-CVD high internal quality-factor ($\approx 10^5$) and compatibility in the magnetic would lead to flux tunable hybrid systems by directly incorporating these resonators in growth processes with carbon nanotubes and nanowires, leading to new research directions^{22,34}.

acknowledgments

The authors would like to thank Prof. Teun Klapwijk, Akira Endo and Pieter de Visser for discussions and help during the measurements. The work was supported by the Dutch Organization for Fundamental Research on Matter (FOM).

* Electronic address: v.singh@tudelft.nl

¹ Lerner, E., Daunt, J. G., and Maxwell, E. *Physical Review* **153**(2), 487–492 January (1967).

² Yasaitis, J. and Rose, R. *IEEE Transactions on Magnetics* **11**(2), 434–436 March (1975).

³ Andreone, A., Barone, A., Di Chiara, A., Mascolo, G., Palmieri, V., Peluso, G., and Scotti di Uccio, U. *IEEE Transactions on Magnetics* **25**(2), 1972–1975 March (1989).

⁴ Leonhardt, T., Carln, J.-C., Buck, M., Brinkman, C. R., Ren, W., and Stevens, C. O. *AIP Conference Proceedings* **458**, 685–690 January (1999).

⁵ Seleznev, V. A., Tarkhov, M. A., Voronov, B. M., Milostnaya, I. I., Lyakhno, V. Y., Garbuz, A. S., Mikhailov, M. Y., Zhigalina, O. M., and Goltsman, G. N. *Superconductor Science and Technology* **21**(11), 115006 November (2008).

⁶ Sundar, S., Sharath Chandra, L. S., Sharma, V. K., Chattopadhyay, M. K., and Roy, S. B. *AIP Conference Proceedings* **1512**(1), 1092–1093 February (2013).

⁷ Aziz, M., Hudson, D. C., and Russo, S. *Applied Physics Letters* **104**(23), 233102 June (2014).

⁸ Day, P. K., LeDuc, H. G., Mazin, B. A., Vayonakis, A., and Zmuidzinas, J. *Nature* **425**(6960), 817–821 October (2003).

⁹ Wallraff, A., Schuster, D. I., Blais, A., Frunzio, L., Huang, R.-S., Majer, J., Kumar, S., Girvin, S. M., and Schoelkopf, R. J. *Nature* **431**(7005), 162–167 September (2004).

- ¹⁰ Palacios-Lalay, A., Nguyen, F., Mallet, F., Bertet, P., Vion, D., and Esteve, D. *Journal of Low Temperature Physics* **151**(3-4), 1034–1042 May (2008).
- ¹¹ Regal, C. A., Teufel, J. D., and Lehnert, K. W. *Nature Physics* **4**(7), 555–560 July (2008).
- ¹² Delbecq, M. R., Bruhat, L. E., Viennot, J. J., Datta, S., Cottet, A., and Kontos, T. *Nature Communications* **4**, 1400 January (2013).
- ¹³ Petersson, K. D., McFaul, L. W., Schroer, M. D., Jung, M., Taylor, J. M., Houck, A. A., and Petta, J. R. *Nature* **490**(7420), 380–383 October (2012).
- ¹⁴ Frey, T., Leek, P. J., Beck, M., Blais, A., Ihn, T., Ensslin, K., and Wallraff, A. *Physical Review Letters* **108**(4), 046807 January (2012).
- ¹⁵ Toida, H., Nakajima, T., and Komiyama, S. *Physical Review Letters* **110**(6), 066802 February (2013).
- ¹⁶ Kubo, Y., Ong, F. R., Bertet, P., Vion, D., Jacques, V., Zheng, D., Drau, A., Roch, J.-F., Auffeves, A., Jelezko, F., Wrachtrup, J., Barthe, M. F., Bergonzo, P., and Esteve, D. *Physical Review Letters* **105**(14) September (2010).
- ¹⁷ Amsss, R., Koller, C., Nbauer, T., Putz, S., Rotter, S., Sandner, K., Schneider, S., Schrambck, M., Steinhauser, G., Ritsch, H., Schmiedmayer, J., and Majer, J. *Physical Review Letters* **107**(6), 060502 August (2011).
- ¹⁸ Huebl, H., Zollitsch, C. W., Lotze, J., Hocke, F., Greifenstein, M., Marx, A., Gross, R., and Goennenwein, S. T. B. *Physical Review Letters* **111**(12), 127003 September (2013).
- ¹⁹ Barends, R., Baselmans, J. J. A., Hovenier, J. N., Gao, J., Yates, S. J. C., Klapwijk, T., and Hoevers, H. F. C. *IEEE Transactions on Applied Superconductivity* **17**(2), 263–266 June (2007).
- ²⁰ Hammer, G., Wuensch, S., Roesch, M., Ilin, K., Crocoll, E., and Siegel, M. *Superconductor Science and Technology* **20**(11), S408 November (2007).
- ²¹ Barends, R., Hortensius, H. L., Zijlstra, T., Baselmans, J. J. A., Yates, S. J. C., Gao, J. R., and Klapwijk, T. M. *Applied Physics Letters* **92**(22), 223502 June (2008).
- ²² Schneider, B. H., Etaki, S., van der Zant, H. S. J., and Steele, G. A. *Scientific Reports* **2** September (2012).
- ²³ Singh, V., Bosman, S. J., Schneider, B. H., Blanter, Y. M., Castellanos-Gomez, A., and Steele, G. A. *Nature Nanotechnology* **9**(10), 820–824 October (2014).
- ²⁴ Megrant, A., Neill, C., Barends, R., Chiaro, B., Chen, Y., Feigl, L., Kelly, J., Lucero, E., Mariantoni, M., OMalley, P. J. J., Sank, D., Vainsencher, A., Wenner, J., White, T. C., Yin,

- Y., Zhao, J., Palmstrm, C. J., Martinis, J. M., and Cleland, A. N. *Applied Physics Letters* **100**(11), 113510–113510–4 March (2012).
- ²⁵ Mattis, D. C. and Bardeen, J. *Physical Review* **111**(2), 412–417 July (1958).
- ²⁶ Phillips, W. A. *Reports on Progress in Physics* **50**(12), 1657 December (1987).
- ²⁷ Gao, J., Daal, M., Vayonakis, A., Kumar, S., Zmuidzinis, J., Sadoulet, B., Mazin, B. A., Day, P. K., and Leduc, H. G. *Applied Physics Letters* **92**(15), 152505 April (2008).
- ²⁸ See supplemental material at [URL will be inserted by AIP] for additional data and details of the chemical vapor deposition process.
- ²⁹ Song, C., Heitmann, T. W., DeFeo, M. P., Yu, K., McDermott, R., Neeley, M., Martinis, J. M., and Plourde, B. L. T. *Physical Review B* **79**(17), 174512 May (2009).
- ³⁰ Bothner, D., Gaber, T., Kemmler, M., Koelle, D., Kleiner, R., Wnsch, S., and Siegel, M. *Physical Review B* **86**(1), 014517 July (2012).
- ³¹ Song, C., DeFeo, M. P., Yu, K., and Plourde, B. L. T. *Applied Physics Letters* **95**(23), 232501 December (2009).
- ³² Bothner, D., Gaber, T., Kemmler, M., Koelle, D., and Kleiner, R. *Applied Physics Letters* **98**(10), 102504 March (2011).
- ³³ Graaf, S. E. d., Danilov, A. V., Adamyan, A., Bauch, T., and Kubatkin, S. E. *Journal of Applied Physics* **112**(12), 123905 December (2012).
- ³⁴ Souquet, J.-R., Woolley, M. J., Gabelli, J., Simon, P., and Clerk, A. A. *arXiv:1408.1128 [cond-mat, physics:quant-ph]* August (2014). arXiv: 1408.1128.

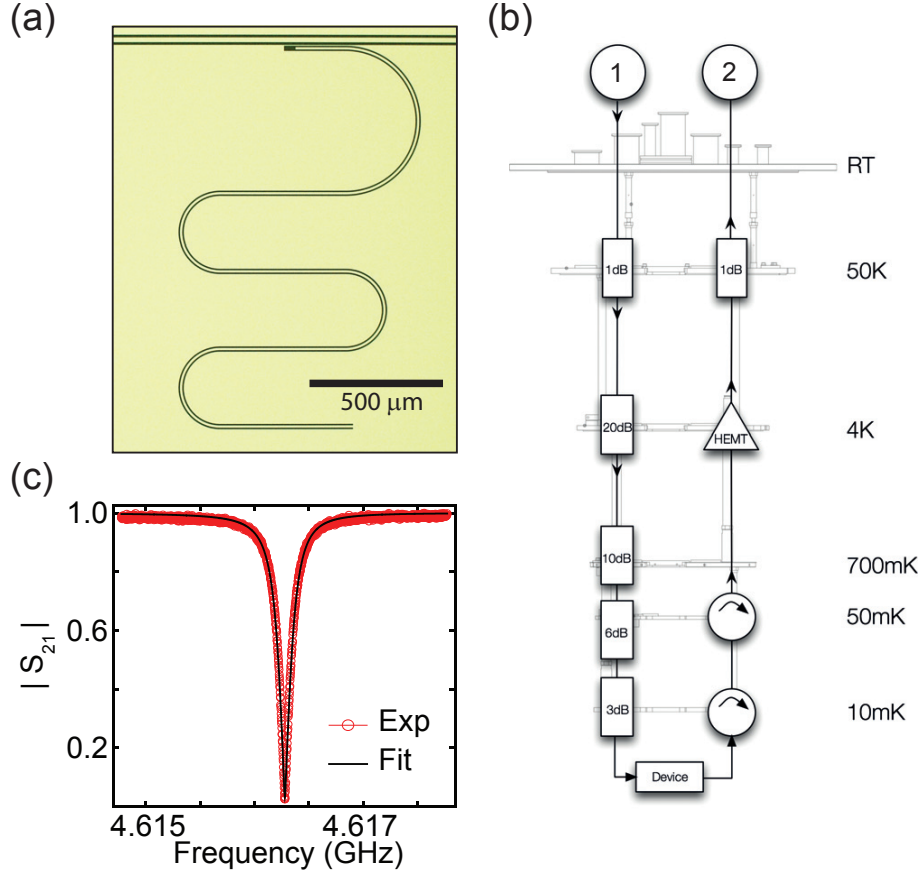


FIG. 1: **Basic device characterization:** (a) False color optical microscope image of a quarter-wavelength resonator side coupled to a transmission line in the coplanar waveguide geometry. The bright region represents the deposited metal and the dark region is the dielectric substrate (sapphire). (b) Schematic of the setup for low temperature measurements. Microwave signal reaching to the device is sufficiently attenuated to equilibrate at various temperature stages. (c) Experimentally measured transmission coefficient $|S_{21}|$ for a resonator at $T = 830$ mK (red circles) with ≈ 100 probe photons. The black curve is the fit to data to extract the resonator parameters yielding $Q_i \sim 700,000$.

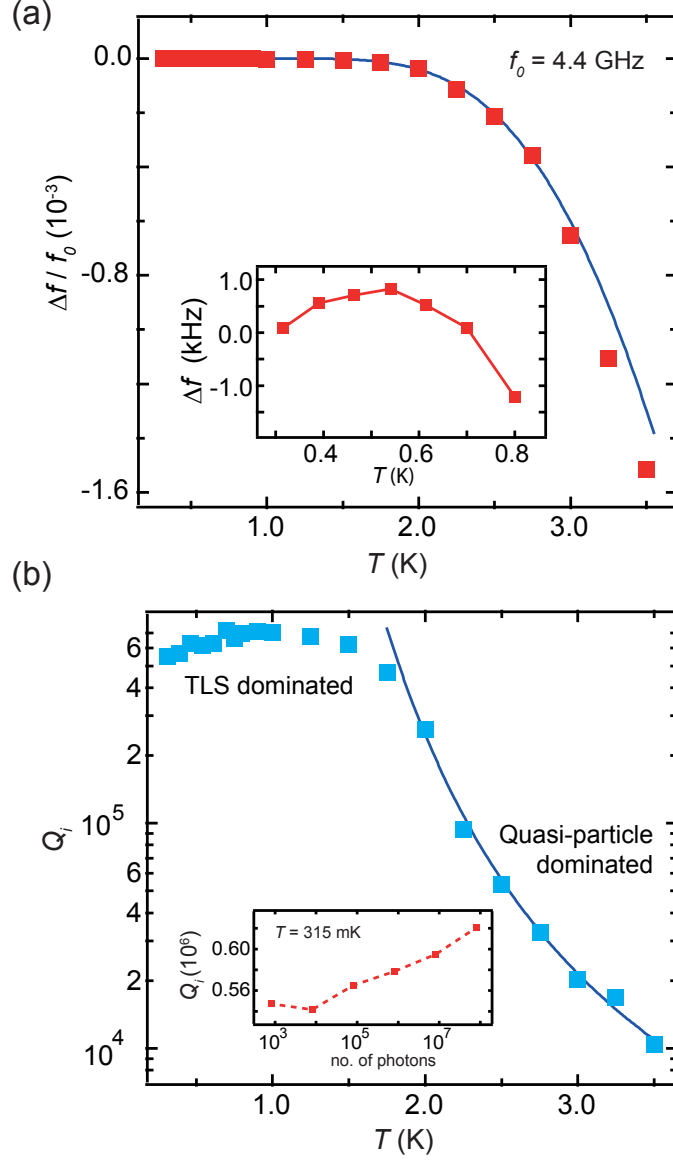


FIG. 2: **Characterization with temperature and identifying the effects of two level systems:** (a) Normalized shift in the resonance frequency of different resonators with temperature. The blue line is the expected behavior from Mattis-Bardeen (M-B) theory (no fit). The inset shows the zoomed-in view of typical resonance frequency shift in the low temperature range. (b) Temperature dependence of the internal quality-factor Q_i at a drive power corresponding to ≈ 1000 photons. The blue line represents the losses due to quasi-particles calculated using M-B theory without any fit parameters. Inset shows the dependence of Q_i with the number of probe photons at $T = 315$ mK suggesting the presence of two level systems.

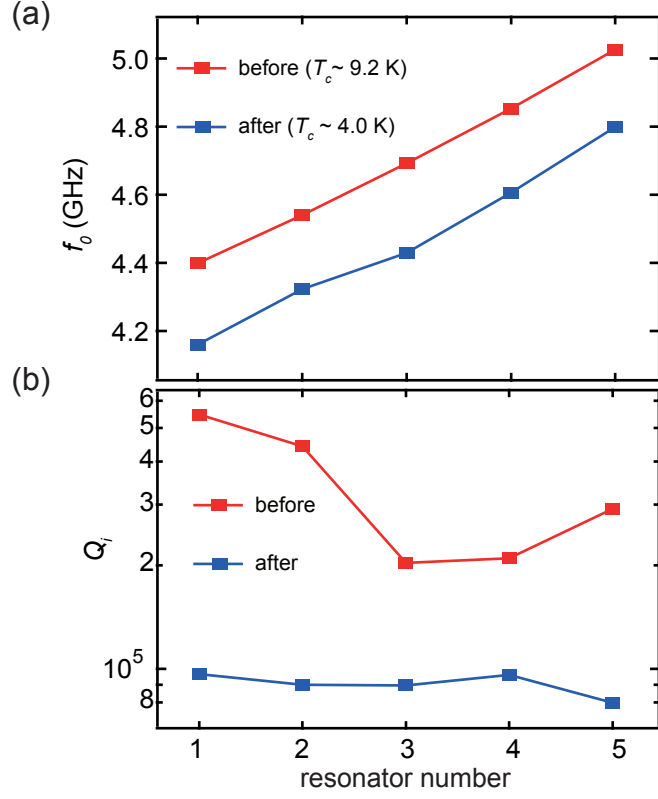


FIG. 3: **Effect of high temperature CVD process on MoRe resonators measured at 315 mK:** Comparison of (a) resonance frequency and (b) internal quality-factors of 5 resonators after first annealing them at 900°C in hydrogen flow and then flowing methane for 10 minutes. After annealing superconducting transition temperature decreases from 9.2 K to 4.0 K and room temperature resistivity changes from $88 \mu\Omega\text{-cm}$ to $108 \mu\Omega\text{-cm}$.

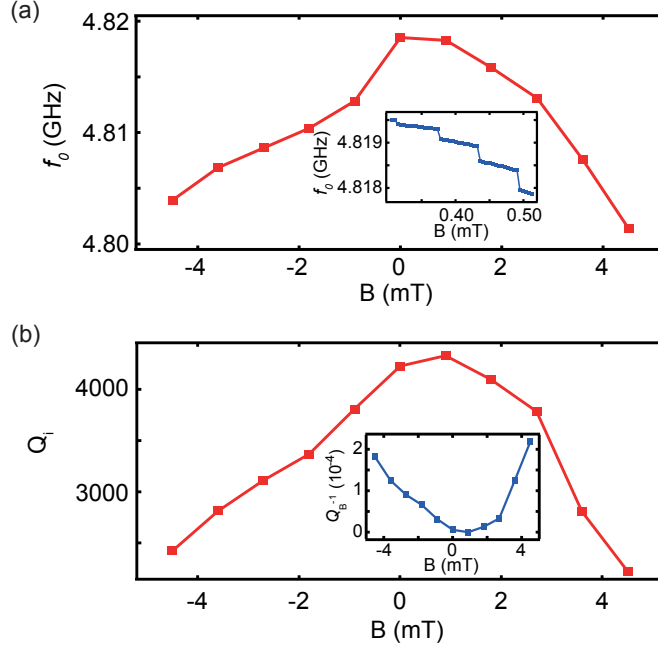


FIG. 4: **Characterization in the magnetic field at 4.2 K:** (a) Plot of resonance frequency with magnetic field at 4.2 K showing a drop in resonance frequency. Inset shows the detailed measurement of resonance frequency (f_0) in a narrow range of magnetic field to highlight the discrete jumps observed in resonance frequency due to the incorporation of vortices. (b) Plot of internal quality-factor Q_i with magnetic field at 4.2 K. The internal quality-factor drops in the presence of magnetic field. Inset shows the magnetic field contribution to the total dissipation in the resonator.

**Supplementary Material : Molybdenum-Rhenium alloy based
high- Q superconducting microwave resonators**

Vibhor Singh,* Ben H. Schneider, Sal J. Bosman, Evert P. J. Merkx, and Gary A. Steele

Kavli Institute of NanoScience, Delft University of Technology,

PO Box 5046, 2600 GA, Delft, The Netherlands.

(Dated: November 19, 2014)

arXiv:1411.4815v1 [cond-mat.mes-hall] 18 Nov 2014

Additional data from other devices:

Figure S1 shows the characterization of additional devices patterned with 180 nm thin film of MoRe. We measured a superconducting transition temperature $T_c \sim 9.2$ K, residual resistance ratio ~ 1.2 . These devices were also measured down to 13 mK. Figure S1(a) shows the temperature dependence of the normalized resonance frequency shift $\Delta f/f_0 = \frac{f_0(T) - f_0(13 \text{ mK})}{f_0(13 \text{ mK})}$ for 10 resonators with resonance frequencies varying from 4.2 GHz to 6.2 GHz. The blue curve shows the expected temperature dependence of the normalized resonance frequency shift calculated using the MB theory with no free parameters, giving surface inductance $L_s \sim 0.41$ pH.

Figure S1(b) shows temperature dependence of the internal quality-factor Q_i for a typical resonator. Internal quality-factors as high as 700,000 are measured at power corresponding to approximately 100 photons at $T = 830$ mK. At lower temperatures, Q_i saturates and follows a trend similar to the normalized resonance frequency shift indicating the presence of the two-level systems (TLS). With large probe photons, damping due to TLS saturate leading to internal quality-factor (as high as 1.1×10^6) as shown in the inset of Figure 1(b). At temperature higher than ~ 1 K, losses due to quasi-particles start to dominate and the internal quality-factor shows an exponential decrease as explained in the main text in details.

Chemical vapor deposition (CVD) process to simulate the growth of the carbon nanotube:

The process involves heating up the sample to 900°C in Argon (1.5 l/min) and hydrogen (700 ml/min) flow. After this, we deactivate the flow of Ar and activate methane (600 ml/min) for 10 minutes while sustaining the temperature at 900°C . The samples were then cooled down to room temperature in hydrogen flow. This process has been used before to grow carbon-nanotubes¹.

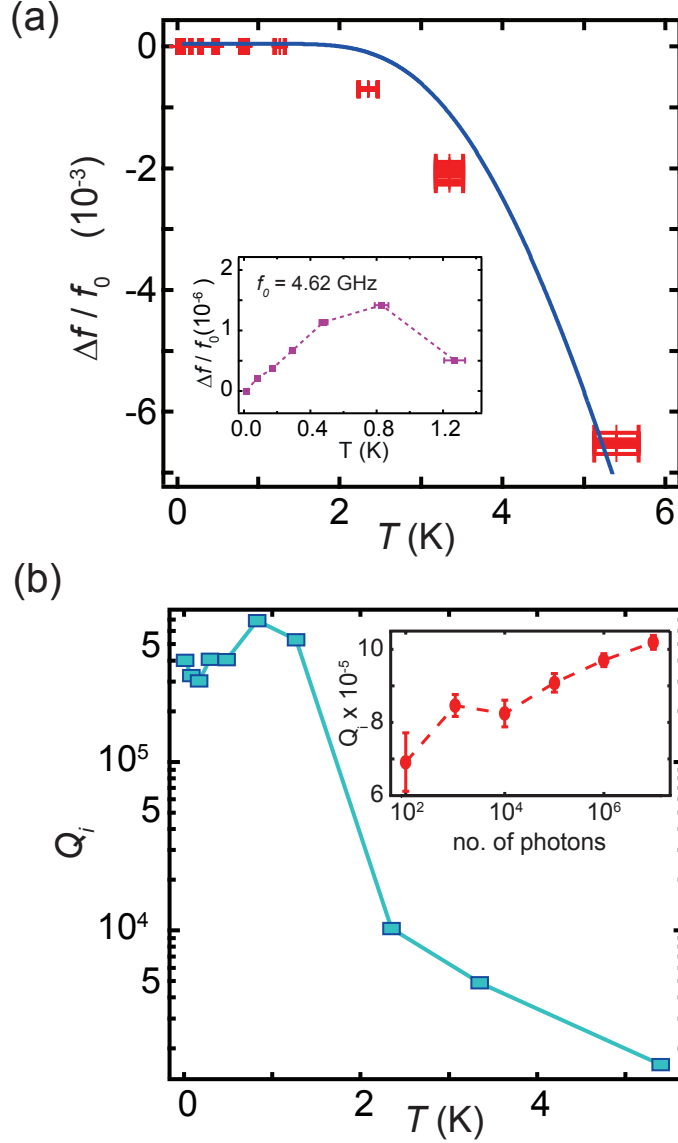


FIG. 1: **Characterization with temperature from an additional device** (a) Normalized shift in the resonance frequency of different resonators with temperature. The blue line is the expected behavior from Mattis-Bardeen theory (no fit). The inset shows the zoomed-in view of typical resonance frequency shift in the low temperature range. (b) Temperature dependence of the internal quality-factor Q_i at a drive power corresponding to ≈ 100 photons. Inset shows the dependence of Q_i with the number of probe photons at $T = 830$ mK suggesting the presence of two level systems.

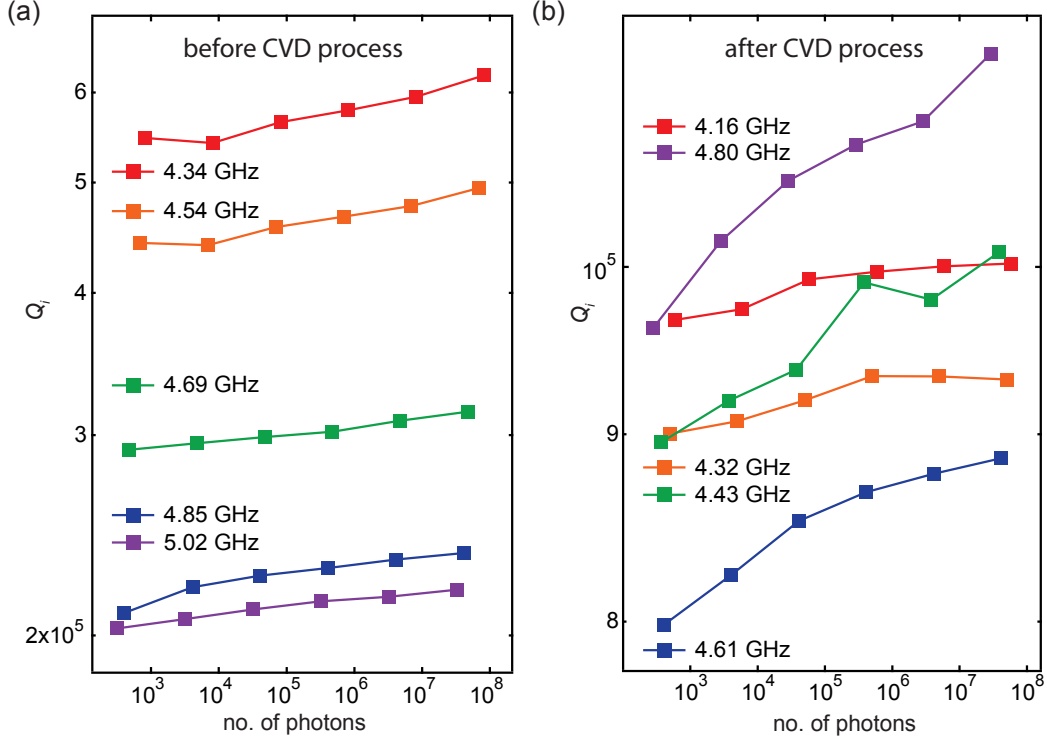


FIG. 2: **Effect of high temperature CVD process on MoRe resonators measured at 315 mK:** Dependence of the internal quality-factor with number of the probe photons before (a) and after (b) the resonator subjected to the process simulating the high temperature chemical vapor deposition carbon nanotube growth process.

Power dependence of the resonator before and after subjecting them to CVD process:

Figure S2 shows the power dependence for 5 resonators before and after subjecting them to CVD growth process for the carbon nanotube. After this process, the superconducting transition temperature reduces to 4.0 K. A sharper change in the internal quality-factor with number of photons after the CVD process and a reduction in T_c suggest an increase in two level system density in the devices.

Effect of annealing in hydrogen flow on resonator properties:

We also studied the effect annealing on the resonators at 900 °C for 30 min in continuous hydrogen flow. After annealing, the superconducting transition temperature T_c of these

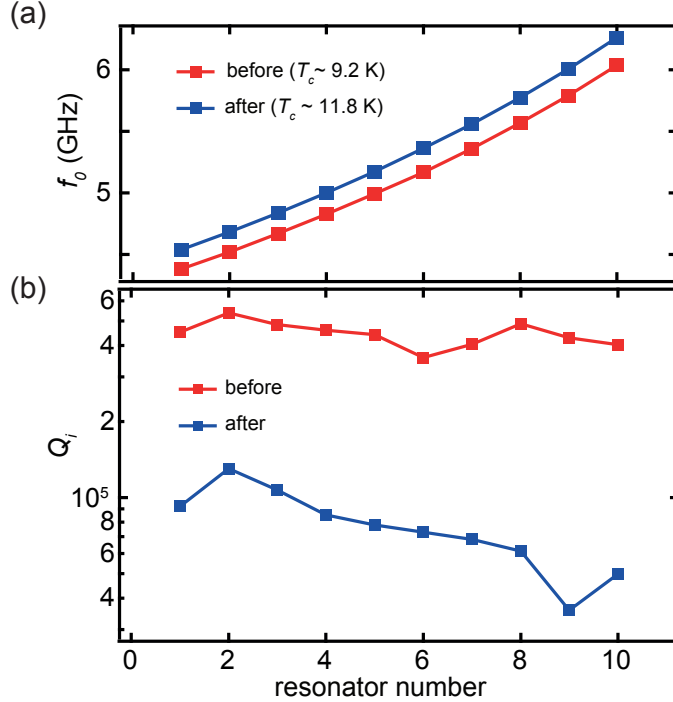


FIG. 3: **Effect of high temperature annealing in hydrogen on MoRe resonators measured at 330 mK:** Comparison of (a) resonance frequency and (b) internal quality-factors of 10 resonators after annealing them at 900°C in hydrogen flow. After annealing superconducting transition temperature increases from 9.2 K to 11.8 K and room temperature resistivity changes from $88 \mu\Omega\text{-cm}$ to $69 \mu\Omega\text{-cm}$.

films increased from 9.2 K to 11.8 K and their RRR improved to ~ 1.9 with a room temperature resistivity of $69 \mu\Omega\text{-cm}$. Such a post-annealing improvement in MoRe thin film quality is consistent with the previous observations with high temperature film deposition². Figure 3 shows a typical change in resonator characteristics before and after high temperature annealing in hydrogen flow measured at 330 mK. For all resonators, we have observed an approximately 150 MHz increase in the resonance frequency after annealing as shown in Figure 3(a). Such an increase in the resonance frequency can be attributed to the reduced kinetic inductance fraction due to the improvement in the superconducting film quality. After annealing, we also observe a reduction in the internal quality-factor of the resonator, shown in Figure 3(b). The larger drop of Q_i after annealing suggests increased dielectric losses in the sapphire substrate. Although the superconducting film quality improves after annealing, the quality of sapphire substrate itself appears to be degraded after annealing,

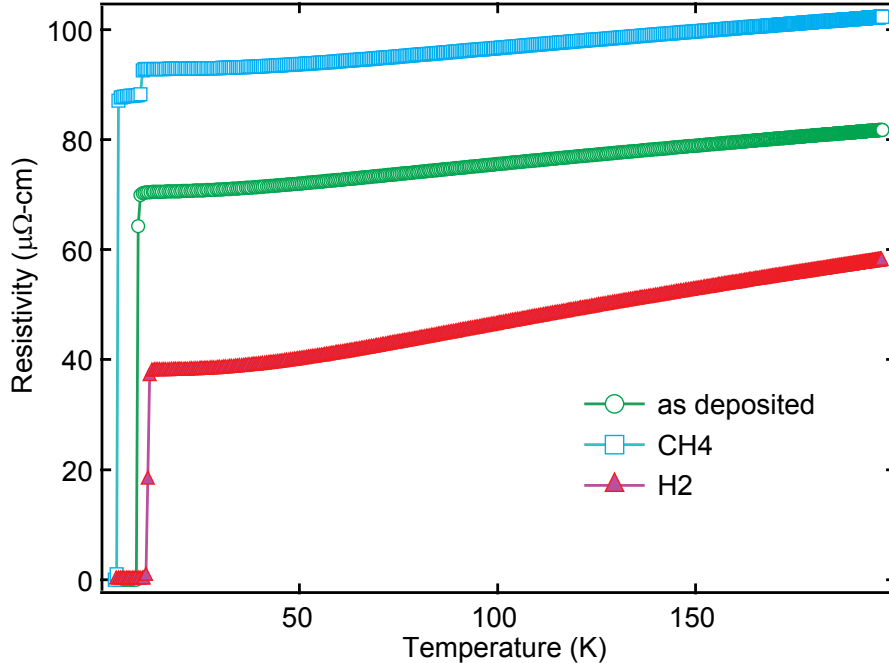


FIG. 4: Plot of the resistivity with temperature for pristine (as deposited) MoRe films, hydrogen annealed MoRe films, and the films simulating the growth of carbon nanotubes with methane.

Process	T_c (K)	RRR	resistivity ($\mu\text{m-cm}$)	Typical Q_i at 300 mK
MoRe (as deposited)	9.2	1.2	88	700,000
MoRe (CVD with methane and hydrogen)	4.0	1.3	108	100,000
MoRe (hydrogen alone)	11.8	1.9	69	100,000

TABLE I: Summary of the results for various processes

resulting in a net decrease of the internal quality-factor of the resonators.

A quick summary:

Figure S4 shows the resistivity at different temperatures for samples with deposited MoRe films, films annealed in hydrogen flow, and films subjected to the CVD growth process described in previous sections. Table I summarizes the key results.

* Electronic address: v.singh@tudelft.nl

¹ Schneider, B. H., Etaki, S., van der Zant, H. S. J., and Steele, G. A. *Scientific Reports* **2** September (2012).

² Testardi, L. R., Hauser, J. J., and Read, M. H. *Solid State Communications* **9**(21), 1829–1831 November (1971).